Motion Planning for Piezo-Actuated Flexible Structures: Modeling, Design, and Experiment

authored by **J. Schröck, T. Meurer, and A. Kugi**

and published in *IEEE Transactions on Control Systems Technology*.

Contact:

Automation and Control Institute (ACIN)
Vienna University of Technology
Gusshausstrasse 27-29/E376
1040 Vienna, Austria

Internet: www.acin.tuwien.ac.at
E-mail: office@acin.tuwien.ac.at
Phone: +43 1 58801 37601
Fax: +43 1 58801 37699

Motion Planning for Piezo-Actuated Flexible Structures: Modeling, Design, and Experiment

Johannes Schröck, Thomas Meurer, *Member, IEEE,* and Andreas Kugi, *Member, IEEE*

***Abstract*—Motion planning and feedforward control is considered for a cantilevered flexible plate-like structure actuated by a finite number of surface-mounted piezoelectric patches to realize prescribed highly dynamic trajectories for the deflection profile in open-loop. For this, a distributed-parameter mathematical model including damping and localized effects originating from the spatially distributed patch actuators is derived by means of the extended Hamilton's principle. With this, a flatness-based design methodology is proposed for motion planning and feedforward control, which directly exploits the distributed-parameter system description. In particular, differential state, input, and output parametrizations are systematically constructed in terms of a basic output to achieve a one-to-one correspondence between system trajectories. Finite element methods are incorporated into the design to account for structures with non-trivial domain and non-isotropic material behavior. In addition, the convergence of the system parametrization is analyzed analytically and by means of numerical results. Finally, measurement results demonstrate the applicability of this approach for the realization of highly dynamic rest-to-rest transitions of the deflection profile of an orthotropic plate structure with macro-fiber composite patch actuators.**

***Index Terms*—Motion planning, feedforward control, flatness, smart structure, flexible structure, piezoelectric actuation, Kirchhoff plate, experimental validation, in-domain control.**

I. Introduction

THE control of flexible structures is a key task in many fields of applications since the trend to increase performance and efficiency by means of lightweight constructions requires to systematically account for the resulting limited structural stiffness. For this reason, vibration control of flexible structures is a widely studied discipline, especially in the fields of aeronautics, robotics, and precision engineering. In this context, so-called smart structures with embedded distributed actuators and sensors have received significant attention. Selected applications in particular comprise adaptive optics, flow control as well as adaptive wing structures [1], [2], [3], [4], [5]. Moreover, the vast progress in material and actuator development allows very promising new fields of research, e.g., in view of dynamic shape control or profile adaption of smart structures.

In order to address these issues, the present contribution considers the motion planning and feedforward control problem for a piezo-actuated flexible plate-like structure to achieve high-speed rest-to-rest transitions between different deflection profiles. The proposed approach directly utilizes the distributed-parameter description of the flexible structure in terms of partial differential equations. In strong contrast to the results on the stabilization problem, see, e.g., [6], only few analytical approaches exist to systematically solve the motion planning problem for distributed-parameter systems. In the case of finite-dimensional flexible structures, different approaches are available utilizing, e.g., input shaping or causal and non-causal model inversion (see for instance [7], [8], [9] and the references therein). Moreover, differential flatness has proven to be a powerful tool for finite-dimensional systems [10]. Roughly speaking, differential flatness denotes the ability to parametrize system states and inputs by a so-called flat output and its time-derivatives up to a certain problem-dependent order. In recent years, this concept has been successfully extended to certain classes of infinite-dimensional systems, see, e.g., [11], [12], [13]. Given flexible structures, selected examples include Euler-Bernoulli beam models [14], [15], [16], Timoshenko beam models [17], [18] and Kirchhoff plate models [19], [20]. Thereby, two different control approaches can be distinguished, namely boundary control and spatially distributed in-domain control. While boundary control is widely studied only few contributions address in-domain control.

In the following, a flatness-based approach for motion planning and feedforward control design is presented for the example of a flexible cantilevered orthotropic plate structure with spatially distributed in-domain actuation as schematically shown in Fig. 1. The structure is built up of glass fibre composite material and a finite number of embedded piezoelectric patch actuators. In order to achieve a highly accurate feedforward tracking control it is necessary to include the local stiffening and damping effects resulting from the spatially distributed patches, which results in a distributed-parameter model with spatially varying parameters. Based on the spectral representation of the equations of motion, the state and input parametrizations are systematically constructed in the operational domain in terms of Weierstrass canonical products, which correspond to differential operators of infinite order in the time domain. Their convergence relies on the system's eigenvalue distribution and properties of the desired flat output trajectory. Hence, by suitably assigning a desired trajectory of the flat output the respective feedforward control directly follows from the evaluation of the input parametrization. In addition, an efficient semi-numerical implementation of the feedforward controller is proposed by making use of a weighted-residual approach. In this way, a rather general design systematics is obtained, which allows to cope with non-trivial spatial domains and non-isotropic material behavior.

Moreover, the contribution is distinguished by the exper-

J. Schröck, T. Meurer, A. Kugi are with the Automation and Control Institute (ACIN), Vienna University of Technology, Gusshausstrasse 27-29/E376, 1040 Vienna, Austria, e-mail: {schroeck,meurer,kugi}@acin.tuwien.ac.at.

Post-print version of the article: J. Schröck, T. Meurer, and A. Kugi, "Motion Planning for Piezo-Actuated Flexible Structures: Modeling, Design, and Experiment", *IEEE Transactions on Control Systems Technology*, vol. 21, no. 3, pp. 807–819, 2012. DOI: 10.1109/TCST.2012.2196043

imental validation of the design. For this, macro-fiber composite (MFC) patches are utilized as actuators. In contrast to the very brittle nature of the common monolithic PZT (lead zirconate titanate) patches, MFCs are composed of rectangular piezoelectric fibers embedded in an epoxy matrix and covered by interdigitated electrodes and thus result in very flexible patches. Additionally, the large input voltage range [-500,+1500] V together with a larger electromechanical coupling coefficient compared to conventional PZT patches allow for higher actuation forces and larger displacements [21]. Similar to PZT patches MFC actuators intrinsically exhibit hysteresis and creep effects. However, as shown in [22], the application of an appropriate hysteresis and creep compensator allows to cancel out these nonlinearities. In this contribution, this operator-based compensator involving Prandtl-Ishlinskii theory is used such that linear piezoelectric material behavior can be assumed (for details, see [22]). As is illustrated in experimental results conducted with the MFC-actuated plate structure, the proposed approach enables the realization of highly dynamic output trajectories for the deflection profile without exciting spurious oscillations. With this, we also demonstrate the possibility to realize smart structures, which enable dynamic shape adaption and hence show the potential to improve accuracy, performance, and efficiency, e.g., in the field of flow control or adaptive optics.

The paper is organized as follows. In Section II, the governing equations of motion are derived for the MFC-actuated flexible plate structure by means of an energy-based modeling approach using the extended Hamilton's principle. Based on the corresponding variational formulation the existence and uniqueness of the solution is verified and a spectral representation of the equations of motion is introduced in Section III. Section IV presents the derivation of the flatness-based motion planning and feedforward control design, which is finally validated by means of simulation and experimental results in Section V.

II. Energy-based modeling

The setup of the piezo-actuated flexible structure under consideration consists of an orthotropic carrier layer (index c) in form of a rectangular cantilevered plate with domain Ω_c and a finite number N_p of surface mounted rectangular MFC patch pairs (index p), as shown in Fig. 1. Each patch pair consists of two symmetrically placed actuators, one on the front side and one on the back side of the carrier layer, respectively. The placement of the k-th patch pair is specified by the spatial actuator characteristics

$$\Lambda_k(x^1,x^2)=\big(h(x_k^1)-h(x_k^1-L_p^1)\big)\,\big(h(x_k^2)-h(x_k^2-L_p^2)\big) \quad (1)$$

where $h(\cdot)$ represents the Heaviside function, (x_k^1,x_k^2) is the position of the lower left corner of the k-th patch pair and L_p^1, L_p^2 denote the patch dimensions, cf. Fig. 1. Subsequently, the deflection of the structure $w(x^1,x^2,t)$ is restricted to pure bending motion in the x^3-direction by applying an asymmetric voltage supply to each actuator pair. Hence, the voltages $\overline{u}^{fs}(t)$ and $\overline{u}^{bs}(t)$ applied to a patch on the front and back side of the carrier layer, respectively, are given by

$$\overline{u}_k^{fs}(t)=u_0+u_k(t),\quad \overline{u}_k^{bs}(t)=u_0-u_k(t). \quad (2)$$

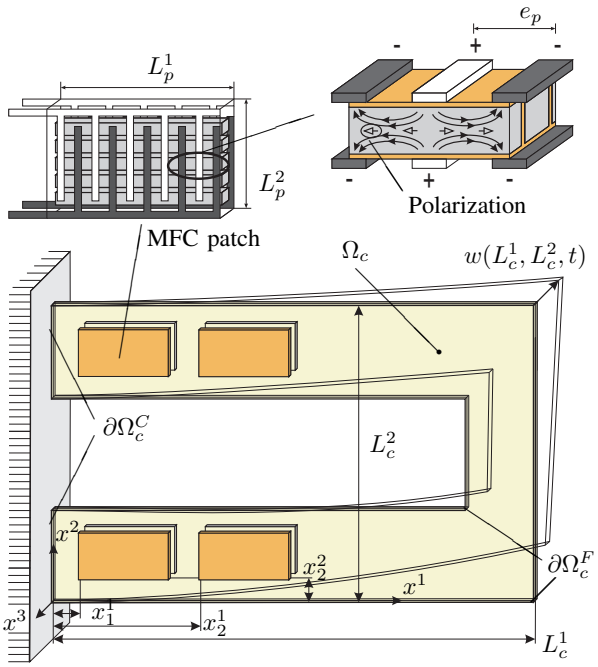

Fig. 1: Schematics of the MFC-actuated plate structure.

The constant supply voltage $u_0 = (u_{\max}+u_{\min})/2$ is used to enable a balanced voltage supply $u_k(t) \in [-\frac{u_{\max}+|u_{\min}|}{2},+\frac{u_{\max}+|u_{\min}|}{2}]$, where $u_{\min}=-500$ V and $u_{\max}=1500$ V are the MFC actuator specific minimal and maximal supply voltages.

A. Equations of motion

The governing equations of motion are derived by applying the extended Hamilton's principle, i.e.

$$\int_{t_0}^{t_e}[\delta W^K-\delta W^P+\delta W^{NC}]\mathrm{d}t=0, \quad (3)$$

where δ denotes the variational operator. The terms $W^K(t)=W_c^K(t)+\sum_{k=1}^{N_p}W_{p,k}^K(t)$ and $W^P(t)=W_c^P(t)+\sum_{k=1}^{N_p}W_{p,k}^P(t)$ represent the kinetic and the potential energy stored in the carrier layer and the MFC patch pairs, respectively, while the virtual work of non-conservative forces due to damping is summarized in the term $W^{NC}(t)=W_c^{NC}(t)+\sum_{k=1}^{N_p}W_{p,k}^{NC}(t)$. The derivation of the respective energy contributions is based on the following assumptions:

A1) rotational inertia is neglected,
A2) the Kirchhoff hypothesis holds,
A3) the constitutive equations of linear elasticity are valid,
A4) all MFC patches are identical, perfectly bonded to the carrier layer, and the adhesive layers are negligible,
A5) the active area of each MFC patch can be characterized by homogenized material parameters reflecting an orthotropic behavior,
A6) the MFC patches show linear piezoelectric material behavior,

Post-print version of the article: J. Schröck, T. Meurer, and A. Kugi, "Motion Planning for Piezo-Actuated Flexible Structures: Modeling, Design, and Experiment", *IEEE Transactions on Control Systems Technology*, vol. 21, no. 3, pp. 807–819, 2012. DOI: 10.1109/TCST.2012.2196043

A7) due to the special arrangement of the interdigitated electrodes the electric field can be approximated by an exclusive homogeneous field strength component $\mathcal{E}_1$ with simultaneously vanishing electric flux density components $D^2 = D^3 = 0$ (cf. Fig. 1), and
A8) the voltage sources are considered to be ideal.

While linear elasticity A3) is a well satisfied property for many materials in case of small strains, it is a matter of common knowledge that piezoelectric materials show intrinsic hysteretic behavior and creep effects [2], [5]. However, the application of an appropriate hysteresis and creep compensator allows to cancel out the nonlinear actuator behavior, see, e.g., [23]. For MFC patch actuators, this is in particular shown by detailed experimental investigations in [22] and hence justifies the validity of assumption A6).

In view of assumption A1) the kinetic energies of the carrier layer and the k-th MFC patch pair are given by

$$\begin{aligned} W_c^K &= \frac{1}{2}\rho_c h_c \int_{\Omega_c} (\partial_t w)^2 \mathrm{d}x^1 \mathrm{d}x^2 \\ W_{p,k}^K &= \rho_p h_p \int_{\Omega_c} \Lambda_k (\partial_t w)^2 \mathrm{d}x^1 \mathrm{d}x^2, \end{aligned} \tag{4}$$

where ρ_c, ρ_p denote the respective mass densities and h_c, h_p represent the thickness of the carrier layer and of the patches. In case of pure bending motion the so-called Kirchhoff strain components ϵ_{ij} depend on the bending deflection $w(x^1, x^2, t)$ in the form $\epsilon_{11} = -x^3 \partial_{x^1}^2 w$, $\epsilon_{22} = -x^3 \partial_{x^2}^2 w$, $\epsilon_{12} = -x^3 \partial_{x^1} \partial_{x^2} w$. For linear elastic orthotropic material behavior the stress-strain relation is given by the constitutive equations

$$\begin{bmatrix} \sigma^{11} \\ \sigma^{22} \\ \sigma^{12} \end{bmatrix} = \begin{bmatrix} c^{1111} & c^{1122} & 0 \\ c^{2211} & c^{2222} & 0 \\ 0 & 0 & c^{1212} \end{bmatrix} \begin{bmatrix} \epsilon_{11} \\ \epsilon_{22} \\ 2\epsilon_{12} \end{bmatrix}, \tag{5}$$

see, e.g., [24], with the stress components denoted by σ^{ij} and the components of the elasticity tensor specified by $c^{1111} = E_1/(1-\nu_{12}\nu_{21})$, $c^{2222} = E_2/(1-\nu_{12}\nu_{21})$, $c^{1122} = c^{2211} = \nu_{12}E_2/(1-\nu_{12}\nu_{21})$, and $c^{1212} = G_{12}$, where E_i, G_{ij} and ν_{ij} with $i, j \in \{1, 2\}$ are Young's moduli, shear moduli, and Poisson's ratio, respectively. Thus, evaluation of the potential energy of the carrier layer yields

$$\begin{aligned} W_c^P &= \int_{V_c} \int_0^t \sigma^{ij} \partial_\tau \epsilon_{ij} \, \mathrm{d}\tau \mathrm{d}V \\ &= \frac{1}{2} I_c \int_{\Omega_c} \Big\{ c_c^1 \left(\partial_{x^1}^2 w\right)^2 + c_c^2 \left(\partial_{x^2}^2 w\right)^2 \\ &\quad + c_c^3 \left(\nabla^2 w\right)^2 + c_c^4 \left(\partial_{x^1} \partial_{x^2} w\right)^2 \Big\} \mathrm{d}x^1 \mathrm{d}x^2, \end{aligned} \tag{6}$$

where V_c denotes the volume of the carrier layer, $I_c = h_c^3/12$, and $c_c^1 = c_c^{1111} - c_c^{1122}$, $c_c^2 = c_c^{2222} - c_c^{1122}$, $c_c^3 = c_c^{1122}$, $c_c^4 = 4c_c^{1212}$.

Based on assumptions A5)-A7) the hysteresis and creep compensated MFC patch actuators can be characterized by the constitutive equations of linear piezoelectricity, i.e.

$$\begin{aligned} \begin{bmatrix} \sigma^{11} \\ \sigma^{22} \\ \sigma^{12} \end{bmatrix} &= \begin{bmatrix} c_p^{1111} & c_p^{1122} & 0 \\ c_p^{2211} & c_p^{2222} & 0 \\ 0 & 0 & c_p^{1212} \end{bmatrix} \begin{bmatrix} \epsilon_{11} \\ \epsilon_{22} \\ 2\epsilon_{12} \end{bmatrix} - \begin{bmatrix} a_1^{11} \\ a_1^{22} \\ 0 \end{bmatrix} D^1, \\ \mathcal{E}_1 &= -\begin{bmatrix} a_1^{11} & a_1^{22} & 0 \end{bmatrix} \begin{bmatrix} \epsilon_{11} \\ \epsilon_{22} \\ 2\epsilon_{12} \end{bmatrix} + \beta_{11} D^1, \end{aligned} \tag{7}$$

see, e.g., [25], with homogenized quantities for the components of the elasticity tensor c_p^{ijfl} and the material parameters a_1^{ii}, β_{11}, with $i, j, f, l \in \{1, 2\}$. With these constitutive equations the potential energy of an MFC patch pair evaluates to

$$\begin{aligned} W_p^P &= \int_{V_p} \int_0^t \left(\sigma^{ij} \partial_\tau \epsilon_{ij} + \mathcal{E}_1 \partial_\tau D^1\right) \mathrm{d}\tau \mathrm{d}V \\ &= \frac{1}{2} \int_{V_p} \left(c_p^{ijfl} \epsilon_{ij} \epsilon_{fl} - 2a_1^{ii} D^1 \epsilon_{ii} + \beta_{11} (D^1)^2\right) \mathrm{d}V, \end{aligned} \tag{8}$$

where V_p represents the sum of the active volumes of the patch located on the front side and the patch located on the back side of the carrier layer. With assumption A8) the third summand in (8) vanishes in the subsequent variational formulation and is hence directly omitted. Furthermore, assuming that the self-generated electric field strength due to the direct piezoelectric effect $-a_1^{ii}\epsilon_{ii}$, cf. (7), is insignificant compared to the applied electric field strength $\mathcal{E}_1$ the electric flux density D^1 can be given in terms of the supply voltage $\overline{u}$, i.e.

$$\int_{x_e^1}^{x_e^1 + e_p} \mathcal{E}_1 \mathrm{d}x^1 = \overline{u} = \beta_{11} D^1 e_p, \tag{9}$$

with e_p denoting the distance between neighboring electrodes, see Fig. 1. Hence, by consideration of the asymmetric voltage supply (2) the potential energy of the k-th patch pair can be rewritten in the form

$$\begin{aligned} W_{p,k}^P &= I_p \int_{\Omega_c} \Lambda_k \Big\{ c_p^1 \left(\partial_{x^1}^2 w\right)^2 + c_p^2 \left(\partial_{x^2}^2 w\right)^2 \\ &\quad + c_p^3 \left(\nabla^2 w\right)^2 + c_p^4 \left(\partial_{x^1} \partial_{x^2} w\right)^2 \Big\} \mathrm{d}x^1 \mathrm{d}x^2 \\ &\quad + \Gamma_{p,k} u_k \int_{\Omega_c} \Lambda_k \Big\{ a_1^{11} \partial_{x^1}^2 w + a_1^{22} \partial_{x^2}^2 w \Big\} \mathrm{d}x^1 \mathrm{d}x^2, \end{aligned} \tag{10}$$

with $I_p = ((h_c/2 + h_p)^3 - (h_c/2)^3)/3$ and $\Gamma_{p,k} = h_p(h_p + h_c)/(\beta_{11} e_p)$.

In order to include damping into the mathematical model the variational derivatives of the virtual works W_c^{NC} and $W_{p,k}^{NC}$ of the non-conservative damping forces are considered in the form

$$\begin{aligned} \delta W_c^{NC} &= -\gamma_c^e \int_{\Omega_c} \partial_t w \delta w \, \mathrm{d}x^1 \mathrm{d}x^2 \\ \delta W_{p,k}^{NC} &= -2\gamma_p^e \int_{\Omega_c} \Lambda_k \partial_t w \delta w \, \mathrm{d}x^1 \mathrm{d}x^2, \end{aligned} \tag{11}$$

with the parameters γ_c^e and γ_p^e referring to viscous (external) damping originating from the carrier layer and the MFC patch pairs, respectively.

Post-print version of the article: J. Schröck, T. Meurer, and A. Kugi, "Motion Planning for Piezo-Actuated Flexible Structures: Modeling, Design, and Experiment", *IEEE Transactions on Control Systems Technology*, vol. 21, no. 3, pp. 807–819, 2012. DOI: 10.1109/TCST.2012.2196043

Finally, evaluation of (3) yields the equations of motion for the MFC-actuated plate structure in the form

$$\begin{aligned}&\rho\partial_t^2 w + \gamma^e\partial_t w + \partial_{x^1}^2\left(I_1\partial_{x^1}^2 w\right) + \partial_{x^2}^2\left(I_2\partial_{x^2}^2 w\right)\\&+\nabla^2\left(I_3\nabla^2 w\right) + \partial_{x^1}\partial_{x^2}\left(I_4\partial_{x^1}\partial_{x^2} w\right) = -\sum_{k=1}^{N_p}\Gamma_k u_k\end{aligned} \tag{12}$$

for $(x^1, x^2, t) \in \Omega_c \times \mathbb{R}^+$ with $\nabla^2 = \partial_{x^1}^2 + \partial_{x^2}^2$. The boundary conditions along the clamped edges $\partial\Omega_c^C$ and the free edges $\partial\Omega_c^F$ are given by

$$w = 0,\ \partial_{x^1} w = 0, \qquad \forall (x^1, x^2) \in \partial\Omega_c^C \tag{13a}$$

$$\left.\begin{aligned}&I_n\partial_{x^n}^2 w + I_3\nabla^2 w = 0\\&\partial_{x^n}\left(I_n\partial_{x^n}^2 w\right)\\&+\partial_{x^n}\left(I_3\nabla^2 w + I_4\partial_{x^\tau}^2 w\right) = 0\end{aligned}\right\} \quad \forall (x^1, x^2) \in \partial\Omega_c^F \tag{13b}$$

with $\nabla^2 = \partial_{x^n}^2 + \partial_{x^\tau}^2$, where the indexes n and τ refer to the normal and the tangential component of the respective boundary. Here, $\rho(x^1, x^2)$, $\gamma^e(x^1, x^2)$, $I_j(x^1, x^2)$, $j = 1, \ldots, 4$, represent spatially varying mass per unit area, viscous damping, and flexural rigidity defined by

$$\begin{aligned}\rho &= \rho_c h_c + 2\sum_{k=1}^{N_p}\Lambda_k\rho_p h_p\\ \gamma^e &= \gamma_c^e + 2\sum_{k=1}^{N_p}\Lambda_k\gamma_p^e\\ I_j &= I_c c_c^j + 2\sum_{k=1}^{N_p}\Lambda_k I_p c_p^j, \quad j = 1, \ldots, 4\end{aligned} \tag{14a}$$

with $c_p^1 = c_p^{1111} - c_p^{1122}$, $c_p^2 = c_p^{2222} - c_p^{1122}$, $c_p^3 = c_p^{1122}$, $c_p^4 = 4c_p^{1212}$ and

$$\Gamma_k = \Gamma_{p,k}\left[a_1^{11}\partial_{x^1}^2\Lambda_k + a_1^{22}\partial_{x^2}^2\Lambda_k\right]. \tag{14b}$$

For the sake of simplicity, zero initial conditions (ICs) are assumed, i.e.

$$w = \partial_t w = 0, \quad t = 0, \tag{15}$$

which, for non-zero stationary ICs, can be obtained by a simple state transformation.

Moreover, a set of reference points $\{(x_{y,j}^1, x_{y,j}^2) \in \Omega_c\}$, $j = 1, \ldots, N_o$, is defined. Hence, let the output of the model be given by $\boldsymbol{y}(t) = [y_1(t), \ldots, y_{N_o}(t)]^T$ with

$$y_j = w|_{(x^1,x^2)=(x_{y,j}^1, x_{y,j}^2)}, \quad j = 1, \ldots, N_o, \tag{16}$$

then the desired motion of the deflection profile $w^d(x^1, x^2, t)$ can be specified by prescribing admissible desired trajectories $t \mapsto y_j^d(t)$ for the individual outputs $y_j(t)$. For the systematic solution of the motion planning problem a spectral approach is subsequently proposed, which utilizes the weak formulation of the equations of motion.

III. Weak formulation and spectral representation

The spatially varying parameters (14) depend on the spatial actuator characteristics (1) such that the strong form of the equations of motion of the MFC-actuated plate structure (12), (13) involves derivatives of the Heaviside function. In order to overcome the necessity to consider distributional solutions the weak or variational form is introduced below.

A. Weak form

Let $\mathcal{V} = H_C^2(\Omega_c) = \{w \in H^2(\Omega_c) \mid w|_{(x^1,x^2)\in\Omega_c^C} = (\partial_{x^1} w)|_{(x^1,x^2)\in\Omega_c^C} = 0\}$ and $\mathcal{H} = L^2(\Omega_c)$ with the inner product on $\mathcal{H}$ given by

$$\left\langle \xi^1, \xi^2 \right\rangle_{\mathcal{H}} = \int_{\Omega_c} \rho\xi^1\overline{\xi^2}\mathrm{d}x^1\mathrm{d}x^2 \tag{17}$$

for $\xi^1(x^1, x^2), \xi^2(x^1, x^2) \in \mathcal{H}$ and $\overline{\xi^2}$ denoting the conjugate complex of ξ^2. Multiplying the mathematical model (12) with a suitable test function $\xi(x^1, x^2) \in H_C^2(\Omega_c)$ and integrating[1] over the domain Ω_c taking into account the boundary conditions (13) yields the weak formulation

$$\begin{aligned}&\left\langle \partial_t^2 w, \xi \right\rangle_{\mathcal{H}} + \sigma_1(w, \xi) + \sigma_2(\partial_t w, \xi)\\&\quad = \left\langle -\frac{1}{\rho}\sum_{k=1}^{N_p} u_k\Gamma_{p,k}\Lambda_k, a_1^{11}\partial_{x^1}^2\xi + a_1^{22}\partial_{x^2}^2\xi \right\rangle_{\mathcal{H}}\end{aligned} \tag{18}$$

with the symmetric sesquilinear forms

$$\begin{aligned}\sigma_1(\xi^1, \xi^2) = \int_{\Omega_c}\Big(&I_1\partial_{x^1}^2\xi^1\overline{\partial_{x^1}^2\xi^2} + I_2\partial_{x^2}^2\xi^1\overline{\partial_{x^2}^2\xi^2}\\&+ I_3\nabla^2\xi^1\overline{\nabla^2\xi^2} + I_4\partial_{x^1}\partial_{x^2}\xi^1\overline{\partial_{x^1}\partial_{x^2}\xi^2}\Big)\mathrm{d}x^1\mathrm{d}x^2\\ \sigma_2(\xi^1, \xi^2) = \int_{\Omega_c}\gamma^e\xi^1\overline{\xi^2}\ \mathrm{d}x^1\mathrm{d}x^2.\end{aligned} \tag{19}$$

The sesquilinear forms exhibit the following properties, which are crucial for the analysis.

Lemma 3.1: The sesquilinear form $\sigma_1(\cdot,\cdot) : \mathcal{V} \times \mathcal{V} \to \mathbb{R}$ is symmetric and $\mathcal{V}$-elliptic, i.e.

(1) $\forall \phi, \psi \in \mathcal{V} : \sigma_1(\phi, \psi) = \overline{\sigma_j(\psi, \phi)}$ (symmetry)
(2) $\exists c_1 \geq 0$ s.t. $\forall \phi, \psi \in \mathcal{V} : |\sigma_1(\phi, \psi)| \leq c_1\|\phi\|_{\mathcal{V}}\|\psi\|_{\mathcal{V}}$ (continuity)
(3) $\exists k_1 > 0$ s.t. $\forall \phi \in \mathcal{V} : \Re(\sigma_1(\phi, \phi)) = \sigma_1(\phi, \phi) \geq k_1\|\phi\|_{\mathcal{V}}^2$

Moreover, $\sigma_2(\cdot,\cdot) : \mathcal{H} \times \mathcal{H} \to \mathbb{R}$ is symmetric and $\mathcal{H}$-elliptic. The proof of Lemma 3.1 is provided in Appendix A-A. Since $\mathcal{V} \hookrightarrow \mathcal{H} = \mathcal{H}' \hookrightarrow \mathcal{V}'$ forms a Gelfand triple with the pivot space $\mathcal{H}$, which can be identified with its dual $\mathcal{H}'$ by the Riesz representation theorem, and $\mathcal{V}'$ the dual of $\mathcal{V}$ the duality pairing $\langle\cdot,\cdot\rangle_{\mathcal{V}',\mathcal{V}}$ can be considered as the continuous extension of $\langle\cdot,\cdot\rangle_{\mathcal{H}}$ on $\mathcal{V}' \times \mathcal{V}$ [2]. The ellipticity of the sesquilinear forms implies the existence of bounded invertible linear operators $\mathcal{A}_j$ by the Lax-Milgram theorem, i.e. $\sigma_j(\xi^1, \xi^2) = \left\langle \mathcal{A}_j\xi^1, \xi^2 \right\rangle_{\mathcal{H}}$, $j = 1, 2$ such that the weak

[1] This requires special attention due to the orientation of the domain to avoid corner conditions.

Post-print version of the article: J. Schröck, T. Meurer, and A. Kugi, "Motion Planning for Piezo-Actuated Flexible Structures: Modeling, Design, and Experiment", *IEEE Transactions on Control Systems Technology*, vol. 21, no. 3, pp. 807–819, 2012. DOI: 10.1109/TCST.2012.2196043

form (18) can be interpreted as an abstract differential equation in $\mathcal{V}'$ according to

$$\partial_t^2 w + \mathcal{A}_1 w + \mathcal{A}_2 \partial_t w = \sum_{k=1}^{N_p} b_k u_k \tag{20}$$

with $b_k u_k(t) \in L^2_{loc}([0,\infty);\mathcal{V}')$ defined by

$$\langle b_k u_k, \xi \rangle_{\mathcal{V}',\mathcal{V}} = \left\langle -\frac{1}{\rho} u_k \Gamma_{p,k} \Lambda_k, a_1^{11}\partial_{x^1}^2 \xi + a_1^{22}\partial_{x^2}^2 \xi \right\rangle_{\mathcal{H}}.$$

Hence, the application of [2, Thm. 4.1] implies the existence and uniqueness of a solution $w(\cdot,\cdot,t)$ of (18) with the regularity properties $w(\cdot,\cdot,t) \in L^2(0,T;\mathcal{V})$, $\partial_t w(\cdot,\cdot,t) \in L^2(0,T;\mathcal{H})$, and $\partial_t^2 w(\cdot,\cdot,t) \in L^2(0,T;\mathcal{V}')$, see, e.g., [26], [2]. Additionally, it can be shown [2, Sec. 4.3] that (20) can be interpreted as an abstract differential equation in $\boldsymbol{\mathcal{V}}_1 = \mathcal{V}_1 \times \mathcal{V}_1$ with $\mathcal{V}_1$ equal to $\mathcal{V}$ but with $\sigma_1(\cdot,\cdot)$ as the inner product, in the form

$$\partial_t \boldsymbol{w} = -\mathcal{A}\boldsymbol{w} + \sum_{k=1}^{N_p} \mathbf{b}_k u_k \tag{21}$$

with $\boldsymbol{w}(t) = [w(\cdot,\cdot,t), \partial_t w(\cdot,\cdot,t)]^T$, $\mathbf{b}_k = [0, b_k]^T$ and the system operator $-\mathcal{A} \in \mathcal{L}(\boldsymbol{\mathcal{V}}_1, \boldsymbol{\mathcal{V}}_1')$ given by

$$-\mathcal{A}\boldsymbol{w} = \begin{bmatrix} 0 & \mathcal{I} \\ -\mathcal{A}_1 & -\mathcal{A}_2 \end{bmatrix} \boldsymbol{w} \tag{22}$$

representing the infinitesimal generator of an analytic C_0-semigroup on $\boldsymbol{\mathcal{H}}_1 = \mathcal{V}_1 \times \mathcal{H}$ as well as on $\boldsymbol{\mathcal{H}} = \mathcal{V} \times \mathcal{H}$ [2, Thm. 4.8]. Here, $\mathcal{I}$ is the identity operator.

B. Spectral representation

The weak form introduced above can be directly utilized to determine the spectral system representation. For this, it is necessary to analyze the eigenproblem $-\mathcal{A}\boldsymbol{\phi}(x^1,x^2) = \lambda\boldsymbol{\phi}(x^1,x^2)$. Contrary to cantilevered Euler-Bernoulli beam models with spatially varying coefficients, see, e.g., [27], no analytic or asymptotic solutions to the eigenproblem are available for the considered plate structure[2]. Hence, the following assumption is imposed.

Assumption 3.1: Let $-\mathcal{A}$ be as above. Then

(A1) $-\mathcal{A}$ is a Riesz-spectral operator in the sense of [30] with isolated point spectrum $(\lambda_n)_{n\in\mathbb{N}}$ and $\lambda_n \neq 0$, $\forall n \in \mathbb{N}$.

(A2) The algebraic and geometric multiplicity r_n and r_n' of λ_n, $n \in \mathbb{N}$ coincide with $r_n < \infty$ and $\sup \Re(\lambda_n) < \infty$.

(A3) The generalized eigenvectors $((\boldsymbol{\phi}_{n_i})_{i=1,\dots,r_n})_{n\in\mathbb{N}}$ and $((\boldsymbol{\psi}_{n_i})_{i=1,\dots,r_n})_{n\in\mathbb{N}}$ of $-\mathcal{A}$ and its adjoint $(-\mathcal{A})^*$ form a biorthogonal Riesz basis for $\boldsymbol{\mathcal{H}}$.

With this, any $\boldsymbol{w}(t) \in \boldsymbol{\mathcal{H}}$ can be represented in terms of the Fourier series

$$\boldsymbol{w} = \sum_{n\in\mathbb{N}} \sum_{i=1}^{r_n} \langle \boldsymbol{w}, \boldsymbol{\psi}_{n_i} \rangle_{\boldsymbol{\mathcal{H}}} \boldsymbol{\phi}_{n_i}. \tag{23}$$

[2]Solutions do exist only for plates with special domains (e.g. circular or rectangular) or special boundary conditions, see, e.g., [28], [29].

Moreover, for any $\lambda \in \varrho(-\mathcal{A})$ with $\varrho(-\mathcal{A})$ denoting the resolvent set of $-\mathcal{A}$ the resolvent operator $R(\lambda,-\mathcal{A}) = (\lambda\mathcal{I} - (-\mathcal{A}))^{-1}$ can be represented as

$$R(s,-\mathcal{A}) = \sum_{n\in\mathbb{N}} \frac{1}{s-\lambda_n} \sum_{i=1}^{r_n} \langle \cdot, \boldsymbol{\psi}_{n_i} \rangle_{\boldsymbol{\mathcal{H}}} \boldsymbol{\phi}_{n_i}. \tag{24}$$

Since $-\mathcal{A}$ is the infinitesimal generator of a C_0–semigroup taking the Laplace transform of (21) yields the spectral representation

$$\hat{\boldsymbol{w}} = \sum_{n\in\mathbb{N}} \sum_{k=1}^{N_p} \frac{\hat{u}_k}{s-\lambda_n} \sum_{i=1}^{r_n} \langle \mathbf{b}_k, \boldsymbol{\psi}_{n_i} \rangle_{\boldsymbol{\mathcal{H}}} \boldsymbol{\phi}_{n_i}. \tag{25}$$

Remark 3.1: The case $r_n' < r_n$ can be treated in a way similar to the presentation above with additional terms arising from the resulting Jordan-like structure. However, this case is outside the scope of this contribution.

IV. Motion planning and feedforward control

Henceforth it is shown that the spectral representation enables the systematic determination of a flat or basic output, which differentially parametrizes the system state, the input, and the output. With this, a very intuitive solution of the motion planning and feedforward control problem is obtained.

A. Flatness-based parametrization

The spectral system representation (25) can be equivalently formulated as

$$\hat{\boldsymbol{w}} = -\sum_{n\in\mathbb{N}} \sum_{k=1}^{N_p} \frac{e^{\mathcal{F}(\frac{s}{\lambda_n},g)} \hat{\mathcal{D}}_n^w(s)}{\hat{\mathcal{D}}^u(s)} \hat{u}_k \sum_{i=1}^{r_n} \frac{\langle \mathbf{b}_k, \boldsymbol{\psi}_{n_i} \rangle_{\boldsymbol{\mathcal{H}}}}{\lambda_n} \boldsymbol{\phi}_{n_i} \tag{26}$$

where

$$\begin{aligned} \hat{\mathcal{D}}_n^w(s) &= \prod_{\substack{l\in\mathbb{N} \\ l\neq n}} \left(1 - \frac{s}{\lambda_l}\right) e^{\mathcal{F}(\frac{s}{\lambda_l},g)}, \\ \hat{\mathcal{D}}^u(s) &= \prod_{l\in\mathbb{N}} \left(1 - \frac{s}{\lambda_l}\right) e^{\mathcal{F}(\frac{s}{\lambda_l},g)} \end{aligned} \tag{27}$$

denote so-called Weierstrass canonical products of genus[3] g of its sequence of zeros $(\lambda_l)_{l\in\mathbb{N}}$ [31]. Herein, $\mathcal{F}(s,g) = 0$ if $g = 0$ or $\mathcal{F}(s,g) = \sum_{j=1}^{g} s^j/j$ if $g \geq 1$. This is a direct extension of the parametrization derived in [32] for an Euler-Bernoulli beam, which is recovered for $g = 0$. This formulation becomes apparent by considering the relationship between Weierstrass canonical products and entire functions. For any sequence $(\lambda_l)_{l\in\mathbb{N}}$ with genus $g \geq 0$ the products $\hat{\mathcal{D}}_n^w(s)$ and $\hat{\mathcal{D}}^u(s)$ converge and define entire functions whose zeros are exactly $(\lambda_l)_{l\in\mathbb{N},\, l\neq n}$ and $(\lambda_l)_{l\in\mathbb{N}}$, respectively. Appendix B provides an analytically treatable example based on the eigenvalue distribution of an isotropic simply supported rectangular plate with $g > 0$, which further endorses the introduced general formulation.

[3]The smallest positive integer g' for which $\sum_{n\in\mathbb{N}} |a_n|^{-g'} < \infty$ with $a_n \neq 0$, $\lim_{n\to\infty} |a_n| \to \infty$ is denoted as $g+1$ and g is the genus of the sequence $(a_n)_{n\in\mathbb{N}}$ [31].

Post-print version of the article: J. Schröck, T. Meurer, and A. Kugi, "Motion Planning for Piezo-Actuated Flexible Structures: Modeling, Design, and Experiment", *IEEE Transactions on Control Systems Technology*, vol. 21, no. 3, pp. 807–819, 2012. DOI: 10.1109/TCST.2012.2196043
The content of this post-print version is identical to the published paper but without the publisher's final layout or copy editing.

This Weierstrass factorized representation enables the introduction of a flat output in the operational domain by substituting $\hat{\xi}_k(s) = \hat{u}_k(s)/\hat{\mathcal{D}}^u(s)$, which with (26) yields

$$\hat{\boldsymbol{w}} = -\sum_{n\in\mathbb{N}}\sum_{k=1}^{N_p} e^{\mathcal{F}(\frac{s}{\lambda_n},g)}\hat{\mathcal{D}}_n^w(s)\hat{\xi}_k \sum_{i=1}^{r_n}\frac{\langle \mathbf{b}_k, \boldsymbol{\psi}_{n_i}\rangle_{\boldsymbol{\mathcal{H}}}}{\lambda_n}\boldsymbol{\phi}_{n_i} \quad (28)$$
$$\hat{u}_k = \hat{\mathcal{D}}^u(s)\hat{\xi}_k.$$

Moreover, note that any entire function can be expanded into a MacLaurin series, i.e.

$$'\mathcal{D}_n^w(s) = e^{\mathcal{F}(\frac{s}{\lambda_l},g)}\hat{\mathcal{D}}_n^w(s) = \sum_{l\in\mathbb{N}} c_l^w s^l$$
$$\hat{\mathcal{D}}^u(s) = \sum_{l\in\mathbb{N}} c_l^u s^l, \quad (29)$$

with $c_0^w = c_0^u = 1$, which converge for all $s \in \mathbb{C}$. Hence, by taking into account that s is the operational equivalent to time differentiation the state and input parametrizations (28) are equivalent to

$$\boldsymbol{w} = -\sum_{n\in\mathbb{N}}\sum_{k=1}^{N_p}({}'\mathcal{D}_n^w(\partial_t)\circ\xi_k)\sum_{j=1}^{r_n}\frac{\langle \mathbf{b}_k, \boldsymbol{\psi}_{n_j}\rangle_{\boldsymbol{\mathcal{H}}}}{\lambda_n}\boldsymbol{\phi}_{n_j} \quad (30a)$$
$$u_k = \mathcal{D}^u(\partial_t)\circ\xi_k, \quad k = 1, ..., N_p. \quad (30b)$$

These computations are so far only formal and rely on the convergence of (30). As is outlined below, the convergence analysis can in principle be reduced to a problem of trajectory planning for the flat output taking into account the eigenvalue distribution, which determines the series coefficients in (29).

B. Convergence analysis

Similar to the treatise in [32] for an Euler-Bernoulli beam and [33] for a diffusion-reaction system with higher-dimensional spatial domain the convergence of $\boldsymbol{w}(t)$ and $u_k(t)$, $k = 1, ..., N_p$ parametrized according to (30) relies on the order and type[4] of ${}'\mathcal{D}_n^w(s)$ and $\hat{\mathcal{D}}^u(s)$. In addition, it is obvious from (30) that necessarily $\xi_k(t) \in C^\infty(\mathbb{R})$. We have the following convergence result, whose proof can be found in Appendix A-B.

Theorem 4.1: Let $(\lambda_n)_{n\in\mathbb{N}}$ be of convergence exponent[5] ν and genus g, then $\hat{\mathcal{D}}^u(s)$ is an entire function of order $\varsigma = \nu$ and genus g. If $\hat{\mathcal{D}}^u(s)$ is of finite type τ, then $u_k(t) = \mathcal{D}^u(\partial_t)\circ\xi_k(t)$ converges uniformly for any $\xi_k(t) \in G_{D,\alpha}(\mathbb{R})$, the Gevrey class[6] of order $\alpha < 1/\varsigma$.

As is shown in [32], [33] a rather similar argument allows to deduce the convergence of ${}'\mathcal{D}_n^w(\partial_t)\circ\xi_k(t)$ for any $n \in \mathbb{N}$. The convergence of the parametrized Fourier series (30a) can be in addition deduced provided that $\sum_{n\in\mathbb{N}}\sum_{j=1}^{r_n}|\sum_{k=1}^{N_p}({}'\mathcal{D}_n^w(\partial_t)\circ\xi_k(t))\langle \mathbf{b}_k, \boldsymbol{\psi}_{n_j}\rangle_{\boldsymbol{\mathcal{H}}}/\lambda_n|^2 < \infty$ holds. The latter obviously depends on the actuator type and location. The explicit proof of these claims is subsequently omitted but makes use of the following assumption, which implies the approximate controllability of (21) according to [35, Thm. 4.2.1].

Assumption 4.1: For all $n \in \mathbb{N}$ the $(r_n \times N_p)$-matrix defined by $[\langle \mathbf{b}_1, \boldsymbol{\psi}_{n_j}\rangle_{\boldsymbol{\mathcal{H}}}, \ldots, \langle \mathbf{b}_{N_p}, \boldsymbol{\psi}_{n_j}\rangle_{\boldsymbol{\mathcal{H}}}]_{j=1,\ldots,r_n}$ is of rank r_n.

The verification of the convergence conditions on the one hand relies on appropriate trajectory assignment for the flat output addressing the Gevrey condition with $\alpha < 1/\varsigma$ and the considered motion planning problem. On the other hand, order and type depend on the zero set of ${}'\mathcal{D}_n^w(s)$ and $\mathcal{D}^u(s)$, which corresponds to the eigenvalue distribution. Both tasks are addressed below.

C. Trajectory assignment

Based on the parametrizations (30), prescribing a suitable desired trajectory $t \mapsto \xi_k^d(t)$ for the flat output $\xi_k(t)$ directly yields the feedforward control $u_k^d(t)$, which is required to track the respective profile $\boldsymbol{w}^d(t) = [w^d(\cdot,\cdot,t), \partial_t w^d(\cdot,\cdot,t)]^T$ and hence the outputs (16). For this, note that the evaluation of (16) with (30) results in

$$y_j = -\sum_{n\in\mathbb{N}}\sum_{k=1}^{N_p}(\mathcal{D}_n^{w\prime}(\partial_t)\circ\xi_k)\sum_{i=1}^{r_n}\frac{\langle \mathbf{b}_k, \boldsymbol{\psi}_{n_i}\rangle_{\boldsymbol{\mathcal{H}}}}{\lambda_n}c_{n_i,j}, \quad (31)$$

where $c_{n_i,j} = \phi_{n_i}(x_{y,j}^1, x_{y,j}^2)$. Obviously, formally prescribing different $\xi_k(t)$ results in different output trajectories $y_j(t)$. Hence, the motion planning problem can be solved indirectly by assigning a suitable desired trajectory $t \mapsto \xi_k^d(t)$, which realizes the desired motion $\boldsymbol{y}^d(t)$. Once $\xi_k^d(t)$ is available the necessary feedforward control directly follows from (30b).

In particular, (31) can be used to realize rest-to-rest motion from $\boldsymbol{y}_s^0 = \boldsymbol{y}(0)$ to $\boldsymbol{y}_s^T = \boldsymbol{y}(T)$ with prescribed transition time T. The corresponding values of the flat output $\boldsymbol{\xi}_s^0 = \boldsymbol{\xi}(0)$ and $\boldsymbol{\xi}_s^T = \boldsymbol{\xi}(T)$ can be directly determined from the output parametrization under steady state conditions, i.e.

$$y_{s,j}^{\{0,T\}} = -\sum_{n\in\mathbb{N}}\sum_{k=1}^{N_p}\xi_{s,k}^{\{0,T\}}\sum_{i=1}^{r_n}\frac{\langle \mathbf{b}_k, \boldsymbol{\psi}_{n_i}\rangle_{\boldsymbol{\mathcal{H}}}}{\lambda_n}c_{n_i,j} \quad (32)$$

for $j = 1, \ldots, N_o$, which directly follows from (31) by making use of the final value theorem of Laplace transform. Assumption 4.1 thereby implies that $\dim\boldsymbol{\xi} = N_p$ independent output trajectories can be assigned. Thus, let $N_o = N_p$ and let the conditions of Theorem 4.1 hold, then (32) represents a linear system of equations for $\boldsymbol{\xi}_s^{\{0,T\}}$. Moreover, it is obvious that the connection of $\boldsymbol{\xi}_s^0$ and $\boldsymbol{\xi}_s^T$ requires $\boldsymbol{\xi}(t)$ to be locally non–analytic at $t \in \{0, T\}$, i.e. $\boldsymbol{\xi}(0) = \boldsymbol{\xi}_s^0$, $\boldsymbol{\xi}(T) = \boldsymbol{\xi}_s^T$ with $\partial_t^n\boldsymbol{\xi}(t) = 0$ at $t = \{0, T\}$ for all $n \geq 1$. In view of Theorem 4.1, it is in addition required that $\alpha > 1$ or $\varsigma < 1$. A trajectory that can be used to fulfill these requirements is given by

$$\xi_k^d(t) = \begin{cases} \xi_{s,k}^0, & t < 0 \\ \xi_{s,k}^0 + \frac{\Delta\xi_{s,k}}{2}\left[1+\tanh\left(\frac{2(\frac{2t}{T}-1)}{(\frac{4t}{T}(1-\frac{t}{T}))^\sigma}\right)\right], & t \in [0,T] \\ \xi_{s,k}^T, & t > T \end{cases} \quad (33)$$

with $\Delta\xi_{s,k} = \xi_{s,k}^T - \xi_{s,k}^0$ and σ determines the slope of the transition function.

[4]For a definition of these notions for entire functions consult [34], [31].

[5]The infimum ν of positive numbers ν' such that $\sum_{n\in\mathbb{N}}|a_n|^{-\nu'} < \infty$ with $a_n \neq 0$ and $\lim_{n\to\infty}|a_n| \to \infty$ is called the convergence exponent of the sequence $(a_n)_{n\in\mathbb{N}}$ [31].

[6]The function $f(t) \in C^\infty(\mathbb{R})$ is in $G_{D,\alpha}(\mathbb{R})$ if there exist $D, \alpha > 0$ such that $\sup_{t\in\mathbb{R}}|\partial_t^n f(t)| \leq D^{n+1}(n!)^\alpha$ for any $n \in \mathbb{N}$. $f(t)$ is entire if $\alpha < 1$, analytic if $\alpha = 1$, and non-analytic if $\alpha > 1$.

Post-print version of the article: J. Schröck, T. Meurer, and A. Kugi, "Motion Planning for Piezo-Actuated Flexible Structures: Modeling, Design, and Experiment", *IEEE Transactions on Control Systems Technology*, vol. 21, no. 3, pp. 807–819, 2012. DOI: 10.1109/TCST.2012.2196043

D. Finite-dimensional realization and implementation

In order to address the computation of the eigenvalue distribution, the weak formulation (18) can be utilized to determine a finite-dimensional approximation of the equations of motion in the sense of weighted residuals [29]. For this, consider the truncated Fourier series (23), i.e.

$$\boldsymbol{w}^{\mathbb{K}} = \sum_{n\in\mathbb{K}} \sum_{i=1}^{r_n} \langle \boldsymbol{w}, \boldsymbol{\psi}_{n_i} \rangle_{\boldsymbol{\mathcal{H}}} \, \boldsymbol{\phi}_{n_i} = \sum_{n\in\mathbb{K}} \sum_{i=1}^{r_n} q_{n_i} \boldsymbol{\phi}_{n_i} \tag{34}$$

with $q_{n_i}(t) = \langle \boldsymbol{w}(t), \boldsymbol{\psi}_{n_i} \rangle_{\boldsymbol{\mathcal{H}}}$, basis functions $\boldsymbol{\phi}_{n_i}(x^1, x^2)$, and the ordered index set $\mathbb{K} = \{0, 1, \ldots, m\}$. Evaluation of the weak formulation (18) by means of the truncated Fourier series with test functions chosen equal to the set of basis functions directly results in a finite-dimensional model representation of the MFC-actuated structure according to

$$\begin{aligned} M\partial_t^2 \boldsymbol{q} + D\partial_t \boldsymbol{q} + K\boldsymbol{q} &= B\boldsymbol{u} \\ \boldsymbol{y}^N &= C\boldsymbol{q}. \end{aligned} \tag{35}$$

Here, $\boldsymbol{q}(t) = [q_{0_1}(t), \ldots, q_{0_{r_0}}(t), \ldots, q_{m_1}(t), \ldots, q_{m_{r_m}}(t)]^T$, $\boldsymbol{u}(t) = [u_1(t), \ldots, u_{N_p}(t)]^T$, and $y_j(t) = w(x^1_{y,j}, x^2_{y,j}, t)$, $j = 1, \ldots, N_o$. The elements of the symmetric $(N \times N)$–matrices

$$\begin{Bmatrix} M \\ D \\ K \end{Bmatrix} = \begin{Bmatrix} M_c \\ D_c \\ K_c \end{Bmatrix} + \sum_{k=1}^{N_p} \begin{Bmatrix} M_{p,k} \\ D_{p,k} \\ K_{p,k} \end{Bmatrix}$$

with $N = \sum_{n\in\mathbb{K}} r_n$ and the elements of the input and output matrices $B \in \mathbb{R}^{N\times N_p}$ and $C \in \mathbb{R}^{N_o \times N}$ are summarized in (36). Note that the explicit computation of the matrix elements relies on the proper selection of the basis functions $\boldsymbol{\phi}_{n_i}(x^1, x^2)$ since the formulation (35), (36) is only valid for basis functions satisfying the natural boundary conditions (13). Hence, basis functions are subsequently chosen equal to the eigenfunctions of the undamped uniform orthotropic carrier structure, which are numerically determined by making use of finite element methods. For this choice the corresponding eigenvalue problem is given by $M\lambda^2\phi + K\phi = 0$, which directly yields the relation

$$\begin{aligned} I_c \int_{\Omega_c} & \left(c_c^1 \partial^2_{x^1} \phi_j \partial^2_{x^1} \phi_l + c_c^2 \partial^2_{x^2} \phi_j \partial^2_{x^2} \phi_l \right. \\ & \left. + c_c^3 \nabla^2 \phi_j \nabla^2 \phi_l + c_c^4 \partial_{x^1} \partial_{x^2} \phi_l \partial_{x^1} \partial_{x^2} \phi_j \right) \mathrm{d}x^1 \mathrm{d}x^2 \\ & = -\lambda_j^2 \rho_c h_c \int_{\Omega_c} \phi_j \phi_l \mathrm{d}x^1 \mathrm{d}x^2. \end{aligned} \tag{37}$$

In addition, the eigenfunctions can be numerically orthogonalized, i.e. $\int_{\Omega_c} \phi_j(x^1, x^2) \phi_l(x^1, x^2) \mathrm{d}x^1 \mathrm{d}x^2 = \delta_{jl}$ with the Kronecker delta δ_{jl}, which allows to significantly reduce the effort to calculate the matrix elements (36). Spatial derivatives of the eigenfunctions are computed using high-order finite-difference schemes.

Based on (35), the state and input parametrizations can be explicitly evaluated by replacing $\mathbb{N}$ with $\mathbb{K}$ and making use of the solution of the algebraic eigenproblem

$$(\overline{M}\lambda + \overline{K})\boldsymbol{\theta} = 0, \tag{38}$$

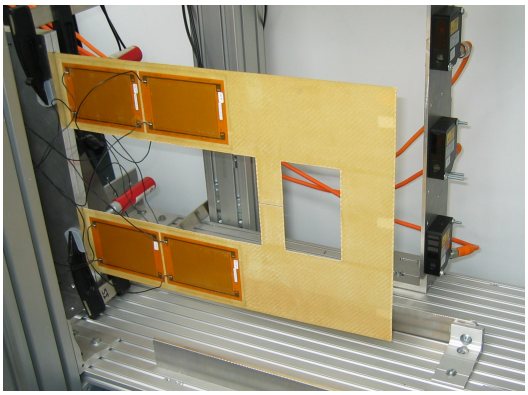

Fig. 2: Picture of the MFC-actuated plate structure.

where $\overline{M} = \left(\begin{smallmatrix} D & M \\ M & 0 \end{smallmatrix}\right)$ and $\overline{K} = \left(\begin{smallmatrix} K & 0 \\ 0 & -M \end{smallmatrix}\right)$ are symmetric $2N \times 2N$ matrices. Since the presented computational procedure can be directly extended to structures with more general geometry, material characteristics, and boundary conditions a very efficient semi–analytical procedure is obtained for the solution of the motion planning and feedforward control problem as is illustrated below for the flexible plate structure.

V. Experimental results

The experimental validation of the proposed feedforward control is performed by means of the flexible plate structure depicted in Fig. 2. The structure is built up of glass fibre composite material with dimensions $L_c^1 = 0.427\,\mathrm{m}$, $L_c^2 = 0.304\,\mathrm{m}$, and $h_c = 0.001\,\mathrm{m}$. The MFC patches are of the type M8557P1 with an active area of dimension $L_p^1 = 85\times10^{-3}\,\mathrm{m}$, $L_p^2 = 57 \times 10^{-3}\,\mathrm{m}$, $h_p = 3 \times 10^{-4}\,\mathrm{m}$, and electrode spacing $e_p = 5 \times 10^{-4}\,\mathrm{m}$ [36]. For each MFC patch pair a separate hysteresis and creep compensator was implemented. In the following, for actuation we solely focus on the patch pairs near the clamped end located at $(x_1^1, x_1^2) = (0.023, 0.021)\,\mathrm{m}$ and $(x_2^1, x_2^2) = (0.023, 0.283)\,\mathrm{m}$. For the verification of the resulting tracking behavior three laser sensors are placed at the positions $(x_{m,1}^1, x_{m,1}^2) = (0.422, 0.012)\,\mathrm{m}$, $(x_{m,2}^1, x_{m,2}^2) = (0.422, 0.152)\,\mathrm{m}$, and $(x_{m,3}^1, x_{m,3}^2) = (0.422, 0.292)\,\mathrm{m}$. The deflection profile of the plate structure is specified by the deflection at the positions $(x_{y,i}^1, x_{y,i}^2) = (x_{m,i}^1, x_{m,i}^2)$ for $i = 1, 3$. The measurements and the implementation of the feedforward tracking control concept are realized using the real-time control board DS1103 of dSPACE with a sampling time of $T_s = 0.2\,\mathrm{ms}$. The power supply is provided by high-voltage power amplifiers PA05039 of Trek Inc. [36].

A. Parameter identification and model validation

The correct determination of the physical parameters of the plate structure is important for the feedforward tracking performance. Since only few parameters are available from data sheets, a parameter identification is performed at the test bench. Due to the incorporation of an appropriate hysteresis and creep compensation the parameters of the resulting linear system can be determined by means of standard identification

Post-print version of the article: J. Schröck, T. Meurer, and A. Kugi, "Motion Planning for Piezo-Actuated Flexible Structures: Modeling, Design, and Experiment", *IEEE Transactions on Control Systems Technology*, vol. 21, no. 3, pp. 807–819, 2012. DOI: 10.1109/TCST.2012.2196043

$$
\begin{aligned}
[M_c]_{j,l} &= \rho_c h_c \textstyle\int_{\Omega_c} \phi_j \phi_l \mathrm{d}x^1 \mathrm{d}x^2 & [M_{p,k}]_{j,l} &= 2\rho_p h_p \textstyle\int_{\Omega_c} \Lambda_k \phi_j \phi_l \mathrm{d}x^1 \mathrm{d}x^2 \\
[D_c]_{j,l} &= \textstyle\int_{\Omega_c} \gamma_c^e \phi_j \phi_l \mathrm{d}x^1 \mathrm{d}x^2 & [D_{p,k}]_{j,l} &= 2 \textstyle\int_{\Omega_c} \Lambda_k \gamma_p^e \phi_j \phi_l \mathrm{d}x^1 \mathrm{d}x^2 \\
[K_c]_{j,l} &= I_c \textstyle\int_{\Omega_c} \big(c_c^1 \partial^2_{x^1} \phi_j \partial^2_{x^1} \phi_l + c_c^2 \partial^2_{x^2} \phi_j \partial^2_{x^2} \phi_l & [K_{p,k}]_{j,l} &= 2 I_p \textstyle\int_{\Omega_c} \Lambda_k \big(c_p^1 \partial^2_{x^1} \phi_j \partial^2_{x^1} \phi_l + c_p^2 \partial^2_{x^2} \phi_j \partial^2_{x^2} \phi_l \\
&\quad + c_c^3 \nabla^2 \phi_j \nabla^2 \phi_l + c_c^4 \partial_{x^1} \partial_{x^2} \phi_l \partial_{x^1} \partial_{x^2} \phi_j \big) \mathrm{d}x^1 \mathrm{d}x^2 & &\quad + c_p^3 \nabla^2 \phi_j \nabla^2 \phi_l + c_p^4 \partial_{x^1} \partial_{x^2} \phi_l \partial_{x^1} \partial_{x^2} \phi_j \big) \mathrm{d}x^1 \mathrm{d}x^2 \\
[C]_{\alpha,i} &= \phi_i|_{(x^1,x^2)=(x^1_{y,\alpha},x^2_{y,\alpha})} & [B]_{i,k} &= \Gamma_{p,k} \textstyle\int_{\Omega_c} \Lambda_k (a_1^{11} \partial^2_{x^1} \phi_i + a_1^{22} \partial^2_{x^2} \phi_i) \mathrm{d}x^1 \mathrm{d}x^2
\end{aligned}
\tag{36}
$$

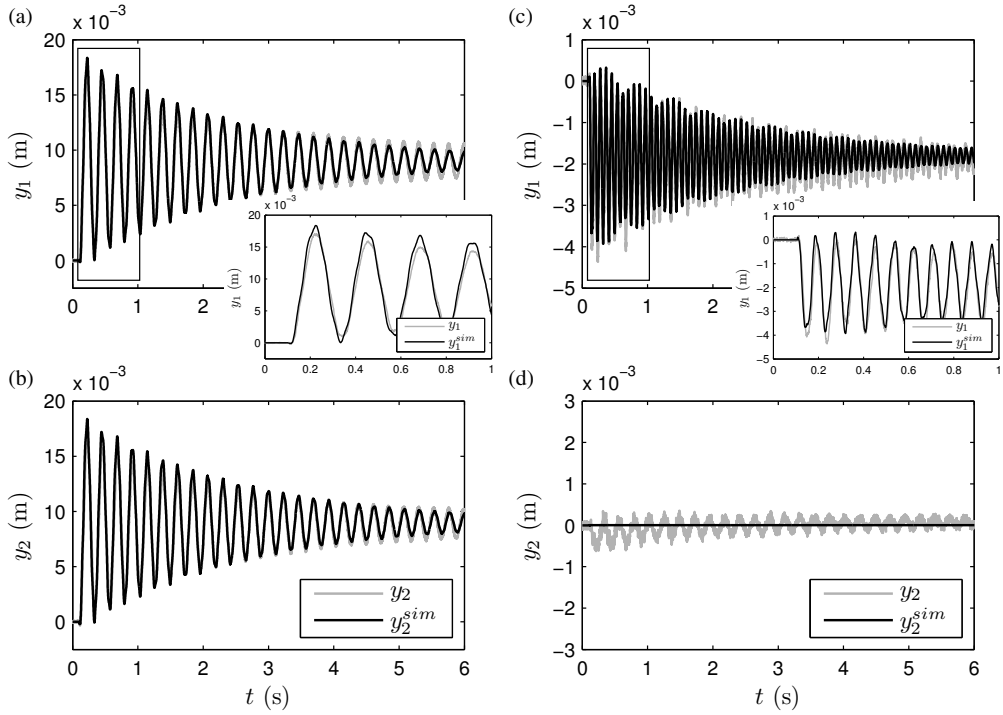

Fig. 3: Comparison of measured $y_i(t)$ and simulated step response $y_i^{sim}(t)$, $i \in \{1,2\}$, at the measurement positions $(x^1_{m,1}, x^2_{m,1}) = (0.422, 0.012)$ m and at $(x^1_{m,2}, x^2_{m,2}) = (0.422, 0.152)$ m. (a), (b) bending motion, (c), (d) twisting motion.

techniques. In particular parameters are identified by minimizing the mean square error between measured and simulated step responses corresponding to bending and twisting motion. The simulation model corresponds to the finite-dimensional approximation (35) with $N = 15$ basis functions, which are calculated by means of the finite element tool ANSYS. However, due to the anisotropy of the carrier structure, which is also reflected in the matrix elements of M, D, and K, the calculation of the eigenfunctions relies on material parameters c_c^{ijfl}. Hence, an iterative procedure has to be considered with a recalculation of the eigenfunctions in each identification step depending on the determined material parameters c_c^{ijfl}. With this, system parameters are obtained as summarized in Table I. To evaluate their validity, Fig. 3 provides a comparison of the simulated and measured step responses, which are in very good agreement both for bending and twisting motion. The minor deviations between the simulated and measured signals depicted in Fig. 3 d) result from an inherent deflection due to the manufacturing process of the plate structure, which causes coupling between the twisting and bending motion not covered by the mathematical model.

B. Motion planning and feedforward control

The finite-dimensional model of the plate structure with parameters identified as specified above serves as the basis for the evaluation of the feedforward controller proposed in Section IV-C. For this, two different rest-to-rest motions of the deflection profile are investigated:

i) bending motion corresponding to the first eigenfunction from $\boldsymbol{y}^d(0) = [y_1^d(0), y_3^d(0)]^T = [0,0]^T$ m to $\boldsymbol{y}^d(T) = [\overline{y}_I, \overline{y}_I]^T$ with $\overline{y}_I \in \{0.005, 0.01\}$ m.

ii) twisting motion corresponding to the second eigenfunction from $\boldsymbol{y}^d(0) = [y_1^d(0), y_3^d(0)]^T = [0,0]^T$ m to $\boldsymbol{y}^d(T) = [+\overline{y}_{II}, -\overline{y}_{II}]^T$ with $\overline{y}_{II} \in \{0.0015, 0.003\}$ m.

The trajectories are chosen according to (33) with a transition time $T = 0.2$ s and $\sigma = 1.8$.

Prior to the experimental validation, the convergence behavior of the parametrizations (30), (31) is investigated by numerical computations. A detailed numerical analysis of the considered plate structure yields mutually disjoint eigenvalues, i.e. $r_n = 1$. In view of the results for the Euler-Bernoulli beam [32] this gives rise to the assumption that also in this

Post-print version of the article: J. Schröck, T. Meurer, and A. Kugi, "Motion Planning for Piezo-Actuated Flexible Structures: Modeling, Design, and Experiment", *IEEE Transactions on Control Systems Technology*, vol. 21, no. 3, pp. 807–819, 2012. DOI: 10.1109/TCST.2012.2196043

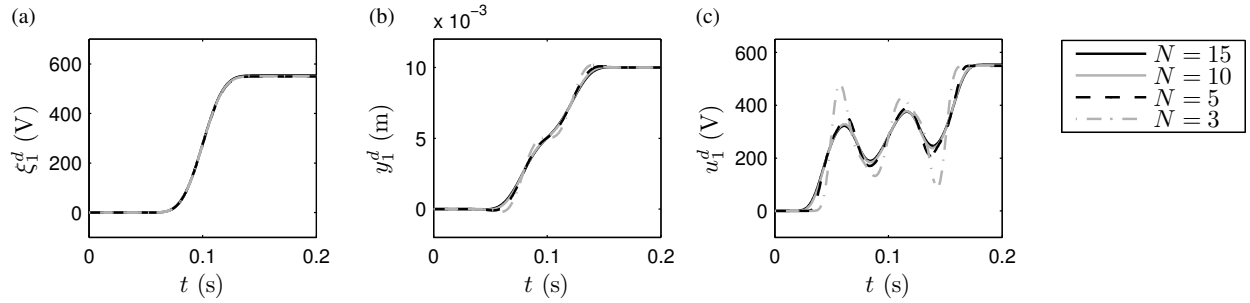

Fig. 4: Convergence of the flatness-based input and output parametrizations for the bending motion: (a) trajectories for the flat output $\xi_1^d(t)$, (b) output trajectories $y_1^d(t)$, and (c) voltage input $u_1^d(t)$.

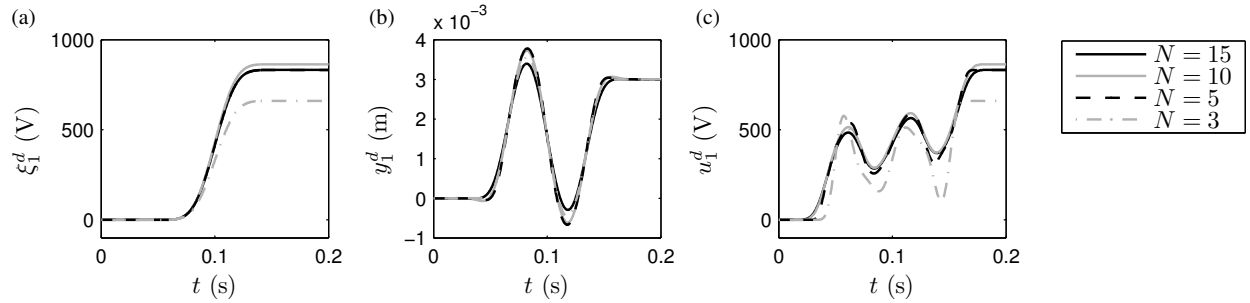

Fig. 5: Convergence of flatness-based input and output parametrizations for the twisting motion: (a) trajectories for the flat output $\xi_1^d(t)$, (b) output trajectories $y_1^d(t)$, and (c) voltage input $u_1^d(t)$.

case $g = 0$. In order to verify this conjecture, the feedforward control for scenarios i) and ii) is calculated with $g = 0$ for an increasing number of basis functions as illustrated in Fig. 4 and Fig. 5, respectively. Thereby, only the voltage trajectory for the first patch pair $u_1^d(t)$ is presented since for the bending motion $u_2^d(t) = u_1^d(t)$ and for the twisting motion $u_2^d(t) = -u_1^d(t)$. It can be deduced that for $g = 0$ the parametrizations for the output $y_1^d(t)$ and the input $u_1^d(t)$ converge with increasing number N of basis functions. Based on these results, subsequently, the feedforward control is determined based on the finite-dimensional model with $N = 15$.

C. Experimental results

The experimental validation is performed for both the bending motion and the twisting motion as defined in the preceding section by scenario i) and ii). In order to illustrate the efficiency of the proposed flatness-based feedforward control, for comparison reasons both scenarios are also realized by using simple transition functions for the voltage signals. Thereby, the input voltages $u_1^d(t)$ and $u_2^d(t)$ are chosen equal to (33) with $\sigma = 1.8$ (cf. Fig. 4 (a)) and suitable start and end values. As it is shown in Fig. 6 (a) and 7 (a) this causes undesirable oscillatory motions which confirms the high flexibility and the low damping of the considered plate structure. However, it can be clearly seen that due to the application of the hysteresis and creep compensator the structure behaves like a weakly damped linear system. In contrast, by means of the proposed flatness-based feedforward control the rest-to-rest motions can be realized in open-loop nearly without exciting spurious oscillations, see Fig. 6 (b) and 7 (b). Note that the transition time of $T = 0.2\,\mathrm{s}$ used in all scenarios is faster than the first eigenfrequency of the structure corresponding to $f_1 = \frac{1}{T_1}$ with $T_1 = 0.23\,\mathrm{s}$. As shown by the corresponding detail views Figs. 6 (c) and 7 (c) the proposed control design allows to realize high-speed rest-to-rest transitions with high tracking accuracy. At this point it should be pointed out that no feedback control is involved and that the presented results are obtained solely by feedforward control. The corresponding voltage signals[7] $\overline{u}_i(t) = \overline{u}_i^{fs}(t) = u_{0,i} + u_i^d(t)$ are presented in the detail views in Figs. 6 (d) and 7 (d). Here, the nominal feedforward control signal corresponding to Figs. 4 (c) and 5 (c), respectively, and the corresponding output of the hysteresis and creep compensator denoted by $\overline{u}_{1,hcc}(t)$ are shown for comparison reasons. The difference between the signals $\overline{u}_1(t)$ and $\overline{u}_{1,hcc}(t)$ demonstrates the adaption of the voltage signal by the compensator to cancel out the hysteresis and creep effects. For further details concerning the hysteresis and creep compensation the interested reader is referred to [22].

VI. Conclusions and Outlook

In this contribution, a systematic approach to motion planning and feedforward control design for flexible structures is presented based on the example of an orthotropic cantilevered elastic plate structure with distributed pairs of MFC patch actuators. By means of an appropriate hysteresis and creep

[7] In order to reduce the inherent deflection resulting from the manufacturing process of the plate structure the values of $u_{0,i} = 500\,\mathrm{V}$, $i = 1, 2$, of the supply voltage $\overline{u}_i^{fs/bs} = u_{0,i} \pm u_i(t)$, cf. (2), are adapted to $u_{0,1}^{fs} = 500 + 100\,\mathrm{V}$, $u_{0,1}^{bs} = 500 - 100\,\mathrm{V}$, $u_{0,2}^{fs} = 500 + 250\,\mathrm{V}$, and $u_{0,2}^{bs} = 500 - 250\,\mathrm{V}$. Furthermore, since there exist only minor differences in the voltage signals $\overline{u}_i^{fs}(t)$ and $\overline{u}_i^{bs}(t)$, in the following only the signals $\overline{u}_i^{fs}(t)$ are shown and the superscript fs is omitted.

Post-print version of the article: J. Schröck, T. Meurer, and A. Kugi, "Motion Planning for Piezo-Actuated Flexible Structures: Modeling, Design, and Experiment", *IEEE Transactions on Control Systems Technology*, vol. 21, no. 3, pp. 807–819, 2012. DOI: 10.1109/TCST.2012.2196043

compensator nonlinear effects resulting from the piezoelectric actuation are canceled out such that the equations of motion are given in terms of the linear Kirchhoff plate equations involving viscous damping with spatially discontinuous parameters due to the distribution of the MFC patches. By the exploitation of a weak or variational form in combination with an appropriate spectral system representation a flat output can be systematically constructed, which allows to differentially parametrize all system variables. Based on this parametrization the motion planning and feedforward control problem is solved by assigning suitable desired trajectories to the flat output. For the explicit evaluation of the proposed feedforward controller a weighted-residual approach is applied to determine a finite-dimensional approximation with basis function computed by incorporating finite element methods to account for the non-trivial domain and the orthotropic material behavior of the plate structure. The convergence of the resulting input and output trajectories is verified numerically. Finally, experimental results demonstrate the applicability of the proposed approach to precisely realize highly dynamic trajectories for the deflection profile of the MFC-actuated plate structure.

Future work is dedicated to the extension of the control design by a feedback controller to realize a two-degree-of-freedom control scheme, which allows to achieve robust trajectory tracking also in case of external disturbances or model uncertainties, see, e.g., [16].

APPENDIX A

A. Proof of Lemma 3.1

The property of symmetry is obviously satisfied. The $\mathcal{V}$-ellipticity of $\sigma_1(\cdot,\cdot)$ is shown in the following. Note that

$$\begin{aligned}|\sigma_1(\phi,\psi)| &= \Bigg| \int_{\Omega_c} \Big(I_1 \partial_{x^1}^2 \phi \overline{\partial_{x^1}^2 \psi} + I_2 \partial_{x^2}^2 \phi \overline{\partial_{x^2}^2 \psi} \\ &\quad + I_3 \nabla^2 \phi \overline{\nabla^2 \psi} + I_4 \partial_{x^1}\partial_{x^2} \phi \overline{\partial_{x^1}\partial_{x^2}\psi} \Big) \mathrm{d}x^1 \mathrm{d}x^2 \Bigg| \\ &\leq c_1 \Bigg(2 \left| \int_{\Omega_c} \partial_{x^1}^2 \phi \overline{\partial_{x^1}^2 \psi} \mathrm{d}x^1 \mathrm{d}x^2 \right| + 2 \left| \int_{\Omega_c} \partial_{x^2}^2 \phi \overline{\partial_{x^2}^2 \psi} \mathrm{d}x^1 \mathrm{d}x^2 \right| \\ &\quad + \left| \int_{\Omega_c} \partial_{x^1}^2 \phi \overline{\partial_{x^2}^2 \psi} \mathrm{d}x^1 \mathrm{d}x^2 \right| + \left| \int_{\Omega_c} \partial_{x^2}^2 \phi \overline{\partial_{x^1}^2 \psi} \mathrm{d}x^1 \mathrm{d}x^2 \right| \\ &\quad + \left| \int_{\Omega_c} \partial_{x^1}\partial_{x^2} \phi \overline{\partial_{x^1}\partial_{x^2} \psi} \mathrm{d}x^1 \mathrm{d}x^2 \right| \Bigg)\end{aligned}$$

with $c_1 = \max(\{\sup_{(x^1,x^2)\in\Omega_c} |I_k(x^1,x^2)|, k = 1,\ldots,4\})$. Furthermore, by means of the Cauchy-Schwarz inequality each summand is bounded, i.e.

$$\begin{aligned}\left| \int_{\Omega_c} \partial_{x^i}^2 \phi \overline{\partial_{x^j}^2 \psi} \mathrm{d}x^1 \mathrm{d}x^2 \right| &\leq \Bigg(\int_{\Omega_c} \left| \partial_{x^i}^2 \phi \right|^2 \mathrm{d}x^1 \mathrm{d}x^2 \times \\ &\quad \int_{\Omega_c} \left| \partial_{x^j}^2 \psi \right|^2 \mathrm{d}x^1 \mathrm{d}x^2 \Bigg)^{1/2} \leq \|\phi\|_{H^2} \|\psi\|_{H^2},\end{aligned}$$

which directly implies

$$|\sigma_1(\phi,\psi)| \leq 7c_1 \|\phi\|_{H^2} \|\psi\|_{H^2} = 7c_1 \|\phi\|_{\mathcal{V}} \|\psi\|_{\mathcal{V}}.$$

Since $\|z\|_{H^p}$ is equivalent to $(\sum_{i+j=p} \|\partial_{x^1}^i \partial_{x^2}^j z\|_{L^2}^2)^{1/2}$, see, e.g., [37], it can be observed that

$$\begin{aligned}\sigma_1(\phi,\phi) &\geq k_1 \Bigg(\int_{\Omega_c} \left| \partial_{x^1}^2 \phi \right|^2 \mathrm{d}x^1 \mathrm{d}x^2 + \int_{\Omega_c} \left| \partial_{x^2}^2 \phi \right|^2 \mathrm{d}x^1 \mathrm{d}x^2 \\ &\quad + \int_{\Omega_c} \left| \partial_{x^1}\partial_{x^2} \phi \right|^2 \mathrm{d}x^1 \mathrm{d}x^2 \Bigg) = k_1 \|\phi\|_{H^2}^2 = k_1 \|\phi\|_{\mathcal{V}}^2\end{aligned}$$

with $k = \min(\{\inf_{(x^1,x^2)\in\Omega_c} I_k(x^1,x^2), k = 1,\ldots,4\}) > 0$. This implies the $\mathcal{V}$-ellipticity of $\sigma_1(\cdot,\cdot)$. Similar results can be obtained for $\sigma_2(\cdot,\cdot)$, i.e.

$$|\sigma_2(\phi,\psi)| = \left| \int_{\Omega_c} \left(\gamma^e \phi \overline{\psi} \right) \mathrm{d}x^1 \mathrm{d}x^2 \right| \leq c_2 \|\phi\|_{\mathcal{H}} \|\psi\|_{\mathcal{H}},$$

with $c_2 = \sup_{(x^1,x^2)\in\Omega_c} \gamma^e(x^1,x^2)$ and $\sigma_2(\phi,\phi) \geq k_2 \|\phi\|_{\mathcal{H}}^2$ with $k_2 = \inf_{(x^1,x^2)\in\Omega_c} \gamma^e(x^1,x^2)$, which verify the $\mathcal{H}$-ellipticity of $\sigma_2(\cdot,\cdot)$.

B. Proof of Theorem 4.1

Since $\hat{\mathcal{D}}^u(s)$ is a Weierstrass canonical product it is an entire function of order equal to the convergence exponent ν of its sequence of zeros $(\lambda_n)_{n\in\mathbb{N}}$ [34, Thm. 2.6.5]. The genus follows from the Hadamard theorem [31, Sec. 4.2]. Moreover, if $\hat{\mathcal{D}}^u(s)$ is of finite type, then there exists a finite $m(\epsilon) \in \mathbb{N}$ s.t. for any $\epsilon > 0$ the coefficients c_l^u of the MacLaurin series expansion satisfy $|c_l^u| \leq [(e\varsigma\tau + \epsilon)/l]^{l/\varsigma}$ for all $l > m(\epsilon)$. Since (30b) is equivalent to $u_k(t) = \sum_{l\in\mathbb{N}} c_l^u \partial_t^l \xi_k(t)$ uniform convergence can be directly deduced from the bound on c_l^u, the Gevrey condition, and the Cauchy-Hadamard theorem.

APPENDIX B

The solution of the eigenvalue problem for an undamped uniform isotropic rectangular plate, simply supported along all four edges, yields isolated eigenvalues in the form

$$\lambda_{m,n} = i\pi^2 \left[\left(\frac{m}{L_c^1} \right)^2 + \left(\frac{n}{L_c^2} \right)^2 \right] \sqrt{\frac{I_c c^{1111}}{\rho_c h_c}} \qquad (39)$$

with $m,n > 0$ [29, Sec. 7.13]. If the ratio of the plate dimensions is rational, i.e. $L_c^1/L_c^2 \in \mathbb{Q}$, multiple eigenvalues exist, e.g., if $L_c^1/L_c^2 = 1$ then $\lambda_{1,2} = \lambda_{2,1}$. Based on (39), it can be shown that the genus of the set of eigenvalues $\{\lambda_{m,n}\}$, i.e. the smallest integer such that

$$S_g = \sum_{m=1}^{\infty} \sum_{n=1}^{\infty} \left[\left(\frac{m}{L_c^1} \right)^2 + \left(\frac{n}{L_c^2} \right)^2 \right]^{-g-1} < \infty, \qquad (40)$$

is given by $g = 1$, cf. Fig. 8, which motivates the operator formulation in (27), (28).

REFERENCES

[1] H. Tzou and G. Anderson, *Intelligent Structural Systems*. Norwell, MA: Kluwer, 1992.

[2] H. Banks, R. Smith, and Y. Wang, *Smart Material Structures: Modeling, Estimation and Control*. Chichester: John Wiley & Sons, 1996.

[3] E. Stanewsky, "Adaptive wing and flow control technology," *Prog. Aerosp. Sci.*, vol. 37, pp. 583–667, 2001.

[4] R. Smith, *Smart Material Systems: Model Development*. Philadelphia: SIAM, 2005.

Post-print version of the article: J. Schröck, T. Meurer, and A. Kugi, "Motion Planning for Piezo-Actuated Flexible Structures: Modeling, Design, and Experiment", *IEEE Transactions on Control Systems Technology*, vol. 21, no. 3, pp. 807–819, 2012. DOI: 10.1109/TCST.2012.2196043

[5] H. Janocha, *Adaptronics and smart structures: basics, materials, design, and applications*, 2nd ed. Berlin, Heidelberg: Springer, 2007.

[6] Z. Luo, B. Guo, and O. Morgül, *Stability and Stabilization of Infinite Dimensional Systems with Applications*. London: Springer–Verlag, 1999.

[7] A. D. Luca, V. Caiano, and D. D. Vescovo, "Experiments on rest–to–rest motion of a flexible arm," in *Experimental Robotics VIII*, B. Siciliano and P. Dario, Eds. Berlin: Springer–Verlag, 2003, vol. 5, pp. 338–349.

[8] G. Clayton, S. Tien, K. Leang, Q. Zou, and S. Devasia, "A Review of Feedforward Control Approaches in Nanopositioning for High–Speed SPM," *J. Dyn. Syst. Meas. Contr.*, vol. 131, no. 6, p. 061101, 2009.

[9] J. Vaughan, A. Yano, and W. Singhose, "Robust Negative Input Shapers for Vibration Suppression," *J. Dyn. Syst. Meas. Contr.*, vol. 131, no. 3, p. 031014, 2009.

[10] M. Fliess, J. Lévine, P. Martin, and P. Rouchon, "Flatness and defect of non–linear systems: introductory theory and examples," *Int. J. Control*, vol. 61, pp. 1327–1361, 1995.

[11] P. Rouchon, "Motion planning, equivalence, and infinite dimensional systems," *Int. J. Appl. Math. Comp. Sc.*, vol. 11, pp. 165–188, 2001.

[12] J. Rudolph, *Flatness Based Control of Distributed Parameter Systems*, ser. Berichte aus der Steuerungs– und Regelungstechnik. Aachen: Shaker–Verlag, 2003.

[13] T. Meurer and M. Zeitz, "Feedforward and feedback tracking control of nonlinear diffusion–convection–reaction systems using summability methods," *Ind. Eng. Chem. Res.*, vol. 44, pp. 2532–2548, 2005.

[14] Y. Aoustin, M. Fliess, H. Mounier, P. Rouchon, and J. Rudolph, "Theory and practice in the motion planning and control of a flexible robot arm using Mikusiński operators," in *Proc. 5th IFAC Symposium on Robot Control*, Nantes (F), 1997, pp. 287–293.

[15] M. Fliess, H. Mounier, P. Rouchon, and J. Rudolph, "Systèmes linéaires sur les opérateurs de Mikusiński et commande d'une poutre flexible," *ESAIM Proceedings*, vol. 2, pp. 183–193, 1997.

[16] T. Meurer, D. Thull, and A. Kugi, "Flatness–based tracking control of a piezoactuated Euler–Bernoulli beam with non–collocated output feedback: theory and experiments," *Int. J. Contr.*, vol. 81, no. 3, pp. 475–493, 2008.

[17] F. Woittennek and J. Rudolph, "Motion planning for a class of boundary controlled linear hyperbolic pde's involving finite distributed delays," *ESAIM: COCV*, vol. 9, pp. 419–435, 2003.

[18] J. Becker and T. Meurer, "Feedforward Tracking Control for Non–Uniform Timoshenko Beam Models: Combining Differential Flatness, Modal Analysis and FEM," *Z. Angew. Math. Mech.*, vol. 87, no. 1, pp. 37–58, 2007.

[19] J. Schröck, T. Meurer, and A. Kugi, "Motion planning for an adaptive wing structure with macro–fiber composite actuators," in *Proc. SPIE Conf. Smart Sensors, Actuators and MEMS*, Dresden (D), May 4-6 2009, pp. 73 621H–73 631H.

[20] T. Meurer and A. Kugi, "Inversion–Based Transient Shaping of a Piezo–Actuated Plate: Motion Planning and Feedforward Control," in *Proc. (CD–ROM) 4th IFAC Symposium on Mechatronic Systems*, Heidelberg (D), Sep. 12–14 2006, pp. 169–174.

[21] R. Williams, G. Park, D. Inman, and W. Wilkie, "An overview of composite actuators with piezoceramic fibers," in *Proc. 20th Modal Analysis Conference*, Los Angeles (CA), USA, February 4-7 2002.

[22] J. Schröck, T. Meurer, and A. Kugi, "Control of a flexible beam actuated by macro-fiber composite patches – Part II: Hysteresis and creep compensation, experimental results," *Smart Mater. Struct.*, vol. 20, no. 1, 2011, article 015016 (11 pages).

[23] K. Kuhnen, "Modeling, identification and compensation of complex hysteretic and log(t)-type creep nonlinearities," *J. Control and Intelligent Systems*, vol. 33, no. 2, pp. 134–147, 2005.

[24] J. Reddy, *Theory and Analysis of Elastic Plates and Shells*, 2nd ed. Taylor & Francis, 2007.

[25] W. Nowacki, *Dynamic Problems of Thermoelasticity*. Warszawa: Noordhoff Int. Publ., PWN–Polish Scientific Publ., 1975.

[26] J. Wloka, *Partial Differential Equations*. Cambridge: Cambridge University Press, 1987.

[27] B.-Z. Guo, "Riesz basis property and exponential stability of controlled Euler–Bernoulli beam equations with variable coefficients," *SIAM J. Control Optim.*, vol. 40, no. 6, pp. 1905–1923, 2002.

[28] A. W. Leissa, *Vibration of Plates*. NASA SP-160, US Government Printing Offices, 1969.

[29] L. Meirovitch, *Principles and Techniques of Vibrations*. New Jersey: Prentice Hall, 1997.

[30] B.-Z. Guo and H. Zwart, "Riesz spectral systems," Faculty of Mathematical Sciences, University of Twente, The Netherlands, Memorandum 1594, 2001.

[31] B. Levin, *Lectures on Entire Functions*. Providence, Rhode Island: American Mathematical Society, 1996.

[32] T. Meurer, J. Schröck, and A. Kugi, "Motion Planning for a Damped Euler–Bernoulli Beam," in *Proc. (CD–ROM) IEEE Conference on Decision and Control (CDC)*, Atlanta (GA), USA, Dec. 15–17 2010, pp. 2566–2571.

[33] T. Meurer, "Flatness–based Trajectory Planning for Diffusion–Reaction Systems in a Parallelepipedon — A Spectral Approach," *Automatica*, vol. 47, no. 5, pp. 935–949, 2011.

[34] R. Boas, *Entire functions*. New York: Academic Press, 1954.

[35] R. Curtain and H. Zwart, *An Introduction to Infinite–Dimensional Linear Systems Theory*, ser. Texts in Applied Mathematics 21. New York: Springer–Verlag, 1995.

[36] "Smart Material Corp." 2010, http://www.smart-material.com.

[37] R. Adams and J. Fournier, *Sobolev Spaces*, 2nd ed. Amsterdam: Acadamic Press, 2003.

Johannes Schröck received the diploma in mechatronics from the Johannes Kepler University (JKU) of Linz, Austria in 2004 and the Ph.D. degree (Dr.techn.) in electrical engineering from Vienna University of Technology, Austria in 2011. His research interests include modeling, simulation, and control of adaptive elasto-mechanical structures, motion planning and feedback control, optimal actuator placement, hysteresis and creep compensation, and piezoelectric actuation.

Thomas Meurer (M'06) received the diploma in chemical engineering from the University of Stuttgart, Germany in 2001 and the M.S. in engineering science and mechanics from the Georgia Institute of Technology, Atlanta, USA in 2000. He received the Ph.D. degree from the University of Stuttgart in 2005. From 2005 to 2007 he was a post-doc with the Chair of System Theory and Automatic Control at the Saarland University in Saarbrücken, Germany, and in 2007 he joined the Automation and Control Institute at the Vienna University of Technology (VUT), Austria, as a senior researcher and as the leader of the distributed–parameter systems group. Since 2012 he is Associate Professor at VUT. His research interests include feedback control and trajectory planning for linear and nonlinear parabolic and hyperbolic distributed–parameter systems, differential flatness, nonlinear control theory, observer design, and computational methods in control. Since 2011 he is Chair of the IFAC Technical Committee 2.6 on Distributed Parameter Systems and serves as Associate Editor for the IFAC Control Engineering Practice.

Post-print version of the article: J. Schröck, T. Meurer, and A. Kugi, "Motion Planning for Piezo-Actuated Flexible Structures: Modeling, Design, and Experiment", *IEEE Transactions on Control Systems Technology*, vol. 21, no. 3, pp. 807–819, 2012. DOI: 10.1109/TCST.2012.2196043

Andreas Kugi received the Dipl.-Ing. degree in electrical engineering from the Technical University of Graz (TU Graz), Austria, in 1992 and the Ph.D. (Dr.techn.) degree in control engineering and the Habilitation degree in the field of automatic control and control theory from the Johannes Kepler University (JKU), Linz, Austria, in 1995 and 2000, respectively. From 1995 to 2000, he was an Assistant Professor and from 2000 to 2002 as an Associate Professor at the JKU. In 2002, he was appointed Full Professor at the Saarland University, Saarbrücken, Germany, where he held the Chair of System Theory and Automatic Control until May 2007. Since June 2007 he has been a Full Professor for Complex Dynamical Systems and head of the Automation and Control Institute, Vienna University of Technology, Austria. He is corresponding member of the Austrian Academy of Science and serves as the Editor-in-Chief of the Control Engineering Practice. His research interests include physics-based modeling and control of (nonlinear) mechatronic systems, differential geometric and algebraic methods for nonlinear control, and control design for infinite-dimensional systems. He is involved in several industrial research projects on automotive applications, hydraulic servo-drives, smart structures, and rolling mill applications.

Post-print version of the article: J. Schröck, T. Meurer, and A. Kugi, "Motion Planning for Piezo-Actuated Flexible Structures: Modeling, Design, and Experiment", *IEEE Transactions on Control Systems Technology*, vol. 21, no. 3, pp. 807–819, 2012. DOI: 10.1109/TCST.2012.2196043

c_c^{1111}	=	4.25×10^{10} Pa	c_p^{1111}	=	1.27×10^{10} Pa	γ_c^e	=	$1.75\,\mathrm{kg/(sm^2)}$
c_c^{2222}	=	17.94×10^{10} Pa	c_p^{2222}	=	2.86×10^{10} Pa	γ_p^e	=	$2.75\,\mathrm{kg/(sm^2)}$
c_c^{1122}	=	5.38×10^{10} Pa	c_p^{1122}	=	1.41×10^{8} Pa	a_1^{11}/β_{11}	=	$5.38\,\mathrm{As/m^2}$
c_c^{1212}	=	8.96×10^{9} Pa	c_c^{1212}	=	2.21×10^{10} Pa	a_1^{22}/β_{11}	=	$-2.06\,\mathrm{As/m^2}$
ρ_c	=	$1732\,\mathrm{kg/m^3}$	ρ_p	=	$5400\,\mathrm{kg/m^3}$			

TABLE I: Parameters for the MFC-actuated plate structure.

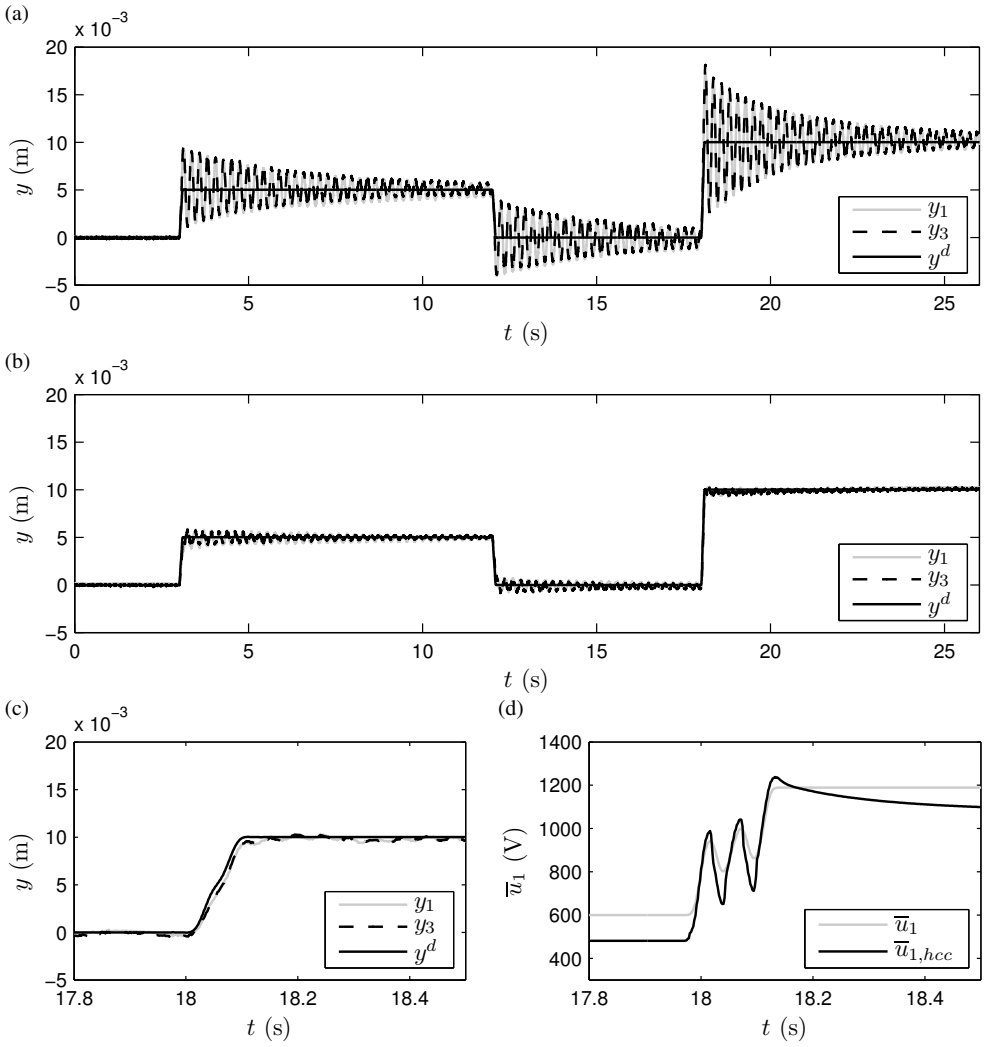

Fig. 6: Rest-to-rest bending motion of the plate structure according to scenario i). Realization with (a) voltage transition function, (b) flatness-based feedforward control, (c) and (d) show detail views of output and applied voltage for (b).

Post-print version of the article: J. Schröck, T. Meurer, and A. Kugi, "Motion Planning for Piezo-Actuated Flexible Structures: Modeling, Design, and Experiment", *IEEE Transactions on Control Systems Technology*, vol. 21, no. 3, pp. 807–819, 2012. DOI: 10.1109/TCST.2012.2196043

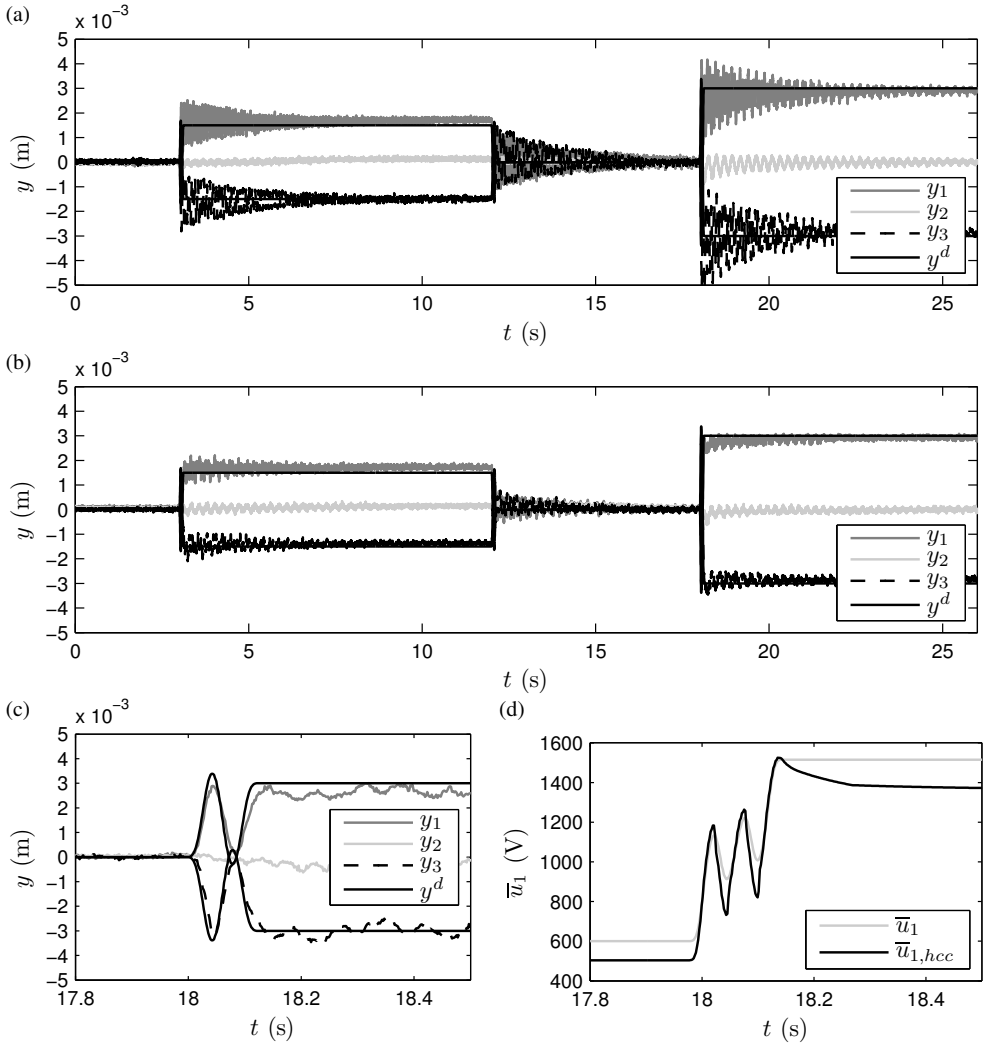

Fig. 7: Rest-to-rest twisting motion of the plate structure according to scenario ii). Realization with (a) voltage transition function, (b) flatness-based feedforward control, (c) and (d) show detail views of output and applied voltage for (b).

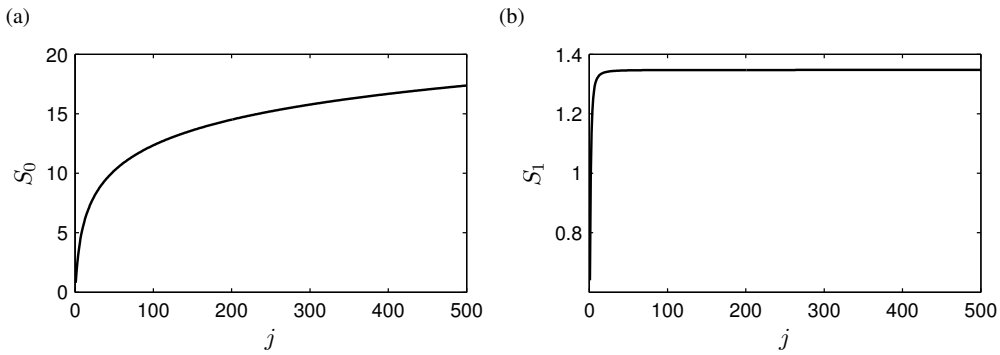

Fig. 8: Series S_g as defined in (40) evaluated for $m, n = 1, \ldots, j$ with $L_c^1 = 1$ and $L_c^2 = 2$. (a) $g = 0$, (b) $g = 1$.

Post-print version of the article: J. Schröck, T. Meurer, and A. Kugi, "Motion Planning for Piezo-Actuated Flexible Structures: Modeling, Design, and Experiment", *IEEE Transactions on Control Systems Technology*, vol. 21, no. 3, pp. 807–819, 2012. DOI: 10.1109/TCST.2012.2196043